DESIGN AND SIZING OF A PARAMETRIC STRUCTURAL MODEL FOR A UCAV CONFIGURATION FOR LOADS AND AEROELASTIC ANALYSIS

A. Voß and T. Klimmek, DLR – German Aerospace Center, Institute of Aeroelasticity, Bunsenstraße 10, D-37073 Göttingen, Germany

Abstract

The set-up of a parametric structural finite element model for loads and aeroelastic analysis of an unmanned combat air vehicle (UCAV) is presented. The DLR-F19 is a “flying wing” configuration with a geometry based on previous research conducted in the scope of the “Mephisto” project and its predecessors “FaUSST” and “UCAV2010”. While there is a considerable amount of knowledge for conventional configurations, unconventional configurations lack of experience, and data for comparison is rarely available. Using an adequate structural model, the conceptual design becomes more sophisticated and allows for the investigation of physical effects already at an early stage of the design process. Strategies for structural modeling and proper condensation, aero-structure coupling, loads integration, control surface attachment, and the use of composite materials are addressed in this paper. The resulting model is sized for minimum structural weight, taking 216 load cases into account. In addition, a comprehensive loads analysis campaign is conducted and resulting loads are evaluated at defined monitoring stations. Next to maneuver loads, quasi-static gust loads are calculated using the Pratt-formula and compared to results obtained from a dynamic 1-cosine gust simulation. The reasons for higher loads when using the Pratt-formula are discussed. The conclusion is that the Pratt formula is suitable for preliminary sizing of “flying wing” configurations.

1. INTRODUCTION

The DLR-F19 is a “flying wing” configuration for an unmanned combat air vehicle (UCAV). The geometry is based on previous research conducted in the scope of the DLR project “Mephisto” and its predecessors “FaUSST” and “UCAV2010” where it was used for wind tunnel investigations (e.g. [1]–[4]) and real sized design concepts (e.g. [5], [6]). While there is a considerable amount of knowledge for conventional configurations, there is little experience for unconventional configurations and data for comparison is rarely available. Some of the few comparable UCAVs are the Northrop Grumman X-47B [7], [8] or Boeing/Nasa X-48 [9], [10] , both experimental demonstrators, while the Northrop B-2 [11], [12] is a much larger stealth bomber. On the civil side and for lower speed, are the Akaflieg Braunschweig SB 13 [13] and Akaflieg Karlsruhe AK-X prototype [14], both sailplanes.

Using an adequate structural model, the conceptual design becomes more sophisticated as it enables detailed loads and aeroelastic analysis such as maneuvering loads, gust encounters or flutter behavior. A comprehensive and detailed level and the use of parametrization allows for the investigation of physical effects already at an early stage of the design process. The importance of such a process is underlined e.g. by companies such as Boeing [15] or Lockheed Martin [16]. Similar processes are developed for wing mass estimations e.g. within Airbus [17], [18]. Other works concentrate on multidisciplinary design and to achieve a feasible and flyable configuration [19]–[21]. This paper concentrates on the challenges imposed by the geometry of the DLR-F19 being significantly different in some aspects from classical aircraft. All this requires different and/or new modelling strategies. The aircraft is much more compact and integrated, so that e.g. established aero structural coupling methods need to be enhanced and loads evaluation gets more complicated. The use of a detailed structrual model instead of a condensed one for the loads calculation increases on the one hand the computational requirements significantly, but leads on the other hand to a more realstic loads distribution, especially in chord direction. Furthermore, investigations on the control surface loads are more

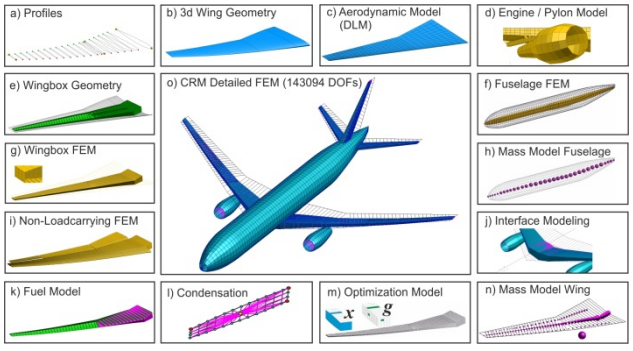

Figure 1: Parametrization concept for simulation and optimization models of the FERMAT configuration [10]

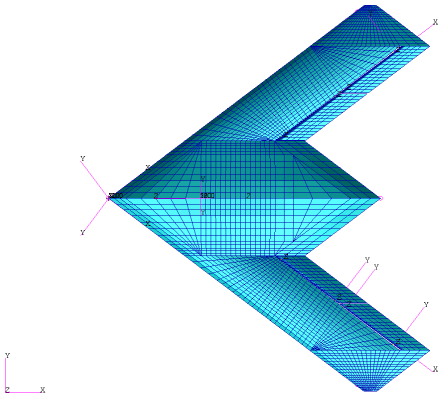

Figure 2: Top view on structural model with local coordinate systems for laminate orientation and the hinge lines of the control surfaces

realistic. Depending on the stability margins, control surface loads are presumably high, because the control surfaces are attached directly to the wing and have therefore rather short lever arms.

The DLR's parametric modelling process is outlined in Section 2. Next, the resulting aeroelastic model is presented in Section 3 and the differences and challenges compared to a classical configuration are discussed. Once the model is set up, a sizing loop is started to minimize the structural weight of the aircraft. The inputs and results are discussed in Section 4. In Section 5, a comprehensive loads analysis is conducted to identify the critical load cases for the DLR-F19 configuration. In addition, dynamic 1-cosine gust calculations are performed and compared to results of the Pratt formula. The latter is used to account for gust loads in the sizing loop.

2. PARAMETRIC MODELLING, LOADS, AND DESIGN PROCESS

To realize such a parametric model, the in-house software ModGen [22] is used. ModGen is a parametrized processor to set up MSC.Nastran finite element models as well as aerodynamic models, optimization models for structural sizing, and other MSC.Nastran simulation models (e.g. for mass modelling). Input to this process is basic information such as profile data, geometrical dimensions and design parameters of the wing box (e.g. number, position and orientation of spars, ribs and stringer). The software has various modules that take care of the individual aircraft components depicted in Figure 1 and creates nearly all data required for various MSC.Nastran calculations, depending on the selected MSC.Nastran solution.

Developed for classical aircraft configurations, not all modules of ModGen are needed for the DLR-F19 (e.g. engine, pylon and fuselage model) while others (e.g. wingbox and mass model) needed to be extended. For example, the rather complex structural topology of the DLR-F19 is a challenge for such an automated process. Therefore, the aircraft is divided into three independent segments: the fuselage region from the center line to the kink, the wing section and the triangular outer wing. There are five spars in the fuselage section with different orientations that eventually merge into only two spars to form the wing box in the wing section. Then, at the outer wing, the two spars continue until they run out at the wing tip. All in all, there are many sharp corners all over the aircraft which lead to meshing challenges if points and edges are not merged or blended properly. This requires very robust algorithms, which needed to be adapted several times to ensure a smooth model generation. In addition, new features were developed for the use of composite material and better support for full, asymmetric models.

ModGen may be used as a stand-alone tool, as part of the ModGen/Nastran design process (MONA) [23], [24] or modules may be integrated in a fully automated design process [5]. The MONA process can be set up slightly different, the principal steps used for the DLR-F19 are depicted in Figure 3. Once the model is generated with ModGen, MSC.Nastran is started to calculate a set of load cases. External load cases may be considered at this step. With the resulting set of loads, a structural sizing is started, based on MSC.Nastran's SOL200. These two steps form an iterative process that may be repeated until convergence is achieved, resulting in a final structural model.

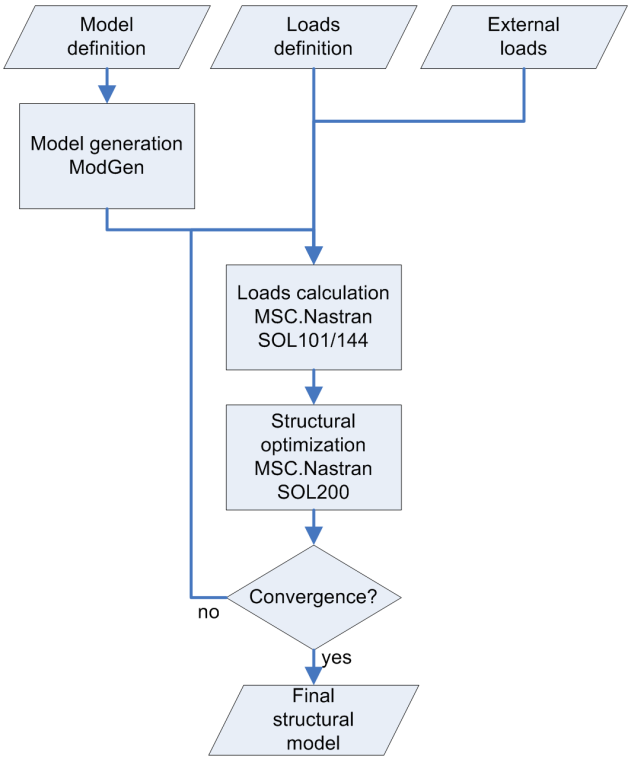

Figure 3: Principal steps of the MONA process used for the DLR-F19

3. SIMULATION MODELS OF THE DLR-F19

3.1. General Aspects

The focus on aeroelastic aspects leads to a number of requirements which differ from a classical finite elements model for stress analysis. The structure should be as realistic as possible because global elastic characteristics such as wing bending and twist are of major interest. Local effects, like stress concentrations at sharp edges ore at holes are neglected. This means that all primary structural components, such as spars, ribs, stringer and skin, should be modelled. In addition to the structural aspects, a mass model with proper distributed mass entities (e.g. structure, systems, payload, fuel) and the consideration of various mass configurations (e.g. fuel, payload) are important to conduct proper dynamic calculations.

As mentioned before, the geometry is based on a given configuration which also served for (scaled) wind tunnel models. The DLR-F19 has a half span of 7.68m and an area of 77m². In a conceptual design process, Liersch and Huber [5] investigated the configuration, established a feasible design and a structural layout.

3.2. Finite Element Model

With this base, a finite element (FE) model with 8054 GRID points and 8578 CQUAD4 and 6326 CBAR elements is created, as shown in Figure 2. A right hand side and a corresponding symmetric left hand side FE model are joined at the center line with RBE2 elements. The spars, ribs and skins are modeled as shell elements and

are equipped with stiffening elements to keep the buckling fields sufficiently small and reduce local eigenmodes. For the stringers, a hat profile is selected.

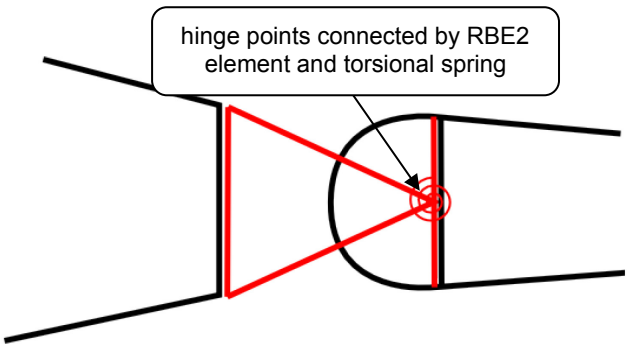

Figure 4: Sketch of elastic control surface attachment to the wing

The control surfaces are structurally modeled as well and attached to the wing elastically. The hinge concept is shown in Figure 4 and consists of two parts. The first part, a triangular beam construction, is mounted on the wing's trailing edge. The second part is a vertical beam at the control surface's first spar, acting as reinforcement. Both parts are designed in such a way, that the two hinge GRID points have exactly the same coordinates. Introducing a torsional spring element, stiffness about the rotation axis defined by a local coordinate system can be placed between these two points while all other degrees of freedom are fixed. The attachment stiffness can be controlled via material properties and the spring's stiffness. This adequate modelling ensures a realistic behavior and allows physically meaningful investigations on control surface loads.

components	laminate setup volume share [0°/±45°/90°]
Skin	40/40/20
Spars	10/80/10
Ribs	10/50/40
Stringer	60/20/20

Table 1: Overview on Chosen Carbon Fiber Laminates

For all structural components, suitable carbon fiber composite properties are chosen, see Table 1. For the skin, the 0° plies are aligned along the leading edge using a local coordinate system to define the orientation. Material properties for unidirectional layers are provided by DLR Institute of Composite Structures and Adaptive Systems [25]. The material properties of the complete laminate setup are calculated as described in [26]. Using the stiffness matrix $\bar{K}_{ij}$ of each layer, the members A_{ij} of the stiffness matrix A of the complete laminate setup are calculated as stated in equation (1). The so-called engineering constants for tensile elasticity $\hat{\mathrm{E}}_x$, $\hat{\mathrm{E}}_y$ and shear G_{xy} are calculated from stiffness matrix A_{ij} and the material thickness t according to equations (2).

$$\frac{A_{ij}}{t} = \sum_{k=1}^{n} \bar{K}_{ij,k} \cdot \frac{t_k}{t} \tag{1}$$

$$\hat{\mathrm{E}}_x = \frac{1}{(A^{-1})_{11} \cdot t}$$

$$\hat{\mathrm{E}}_y = \frac{1}{(A^{-1})_{22} \cdot t} \tag{2}$$

$$G_{xy} = \frac{1}{(A^{-1})_{66} \cdot t}$$

In order to reduce the size of the structural model, a condensation is often used for loads analysis tasks. In addition to the reduced computational costs, the model is also cleaned of modelling shortcomings and undesired effects such as unrealistic local deformations due to high nodal loads. However, for flying wing configurations, such a condensation is not as straight forward as for classical configurations. The use of a loads reference axis is a good approach in the case of slender components like a classical aircraft wing, but appears to be less suitable in the case of a compact, non-slender configuration such as the DLR-F19. Based on these considerations, it was decided to stay with the full model and to accept possible disadvantages.

3.3. Mass Model

Proper mass modelling and the consideration of various mass configurations is important for an aeroelastic model. Due to the material density and dimensions, the structural mass is already included in the FE model. All non-structural masses are added in a separate mass model as so-called condensed or lumped masses, depicted in Figure 5. The individual mass items are connected to the surrounding structure using of RBE3 elements. From the huge amount of possible mass combinations, five distinct mass configurations are selected, shown in Table 2. Neither payload nor fuel level change the center of gravity significantly.

Key	Description	Mass [kg]	CG_x [m]	MAC [%]
-	structure only, no systems	2756	6.78	48
M1	no fuel, no payload	7361	5.72	30
M2	max. fuel, no payload	12509	5.63	28
M3	max. fuel, max. payload	14509	5.60	28
M4	no fuel, max. payload	9361	5.65	29
M5	half fuel, max. payload	11941	5.61	29

Table 2: Selected Mass Configurations

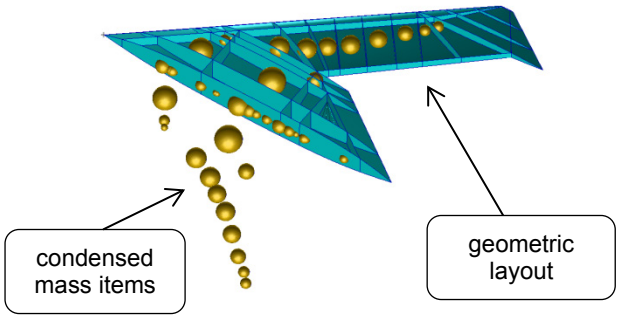

Figure 5: Overview of Mass Model

3.4. Aerodynamic Model

For the aerodynamics, the classical approach using MSC.Nastran's Doublet Lattice Method (DLM) [27] is chosen. The panels are arranged in such a way that 20 panels are defined in flow direction, leading to a total of 840 panels, shown in Figure 6. This discretization is sufficient for static applications but might need to be refined to capture unsteady effects in dynamic calculations. To ensure trapezoidal panels, the pointed wing tip is covered with aerodynamic panels only up to 90%. The DLM is based on a matric of aerodynamic influence coefficients (AIC), which depends on the Mach number Ma and reduced frequency k, with $k = 0$ for the static case. The AIC matrix then relates an induced downwash w_j on each aerodynamic panel to a pressure coefficient cp as stated in equation (3).

$$\{\Delta cp\} = AIC(Ma, k) \cdot \{w_j\} \tag{3}$$

The four control surfaces (AIL-S1, AIL-S2, AIL-S3, AIL-S4, shown in Figure 6) consist of 5x5 panels each and their deflection is modeled by changing the induced downwash due to the rotation about their hinge lines.

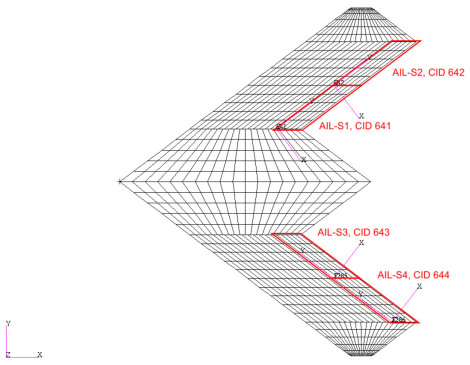

Figure 6: Aerodynamic Mesh and Control Surfaces

3.5. Coupling Strategies

For the coupling of aerodynamic forces with the aircraft structure, a transformation matrix T_{kg} is defined which relates displacements of the structure u_g to displacements of the aerodynamic grid u_k, see formula (4). In addition, as in formula (5), the transposed matrix T_{kg}^T transforms forces and moments from the aerodynamic grid to the structure.

$$\{u_k\} = T_{kg} \cdot \{u_g\} \tag{4}$$

$$\{F_g\} = T_{kg}^T \cdot \{F_k\} \tag{5}$$

There are many possibilities available to create the transformation matrix T_{kg}. One common option is to use a rigid body spline that relates every aerodynamic panel to the closest GRID point on the structure. However, this may result in high nodal forces when using a rather fine structural model. Therefore, surface splines are used, which distribute the aerodynamic forces more evenly to the structural points. To create such a surface spline for coupling, it is decided to use only a subset of structural points on the upper side of the aircraft. In contrast to CFD (computational fluid dynamic) methods like the DLR Tau code [28], the DLM provides only a Δcp between upper and lower side. Aerodynamic forces are usually higher on the suction side. For the spline, the Harder-Desmarais Infinite Plate Spline (IPS) [29] is selected, which is implemented in MSC.Nastran's surface spline SPLINE1. The IPS delivers robust results.

By using a single surface spline for the whole aircraft, challenges arise for example at the control surfaces. Aerodynamic forces on the control surface should act on the structure of the control surface only. This is difficult with a spline that somehow blurs forces and moments and would require component-wise splining. Due to the application of an interpolation method and the use of different discretizations (structure and aerodynamic), a similar phenomenon occurs when integrating the forces and moments of the structural points to calculate section forces. The structural points can be defined clearly, but the origin of the aerodynamic forces acting on them is unknown, making the section forces somewhat imprecise.

4. SIZING

4.1. Load Cases And Design Speeds

For the sizing of the components of the structural model, load cases from three different areas of interest are considered:

- maneuvering loads
- gust loads
- landing loads

Normally, many different types of maneuvers are to be considered, such as pull-up, pull-down, roll or yaw. Due to insufficient control about the vertical axis, only symmetrical manoeuvers are considered, e.g. 1g horizontal flight, 2.5g pull-up and -1.0g push-down. For dive speed V_d/ M_d, the push-down is reduced to 0.0g. The applied set of maneuvers is in close relation to the maneuvers required by the certification specifications CS-25 for large transportation aircraft [30]. In the context of a collaboration between DLR and Airbus Defence and Space as part of the Mephisto project, the loads department defined a set of additional aircraft response parameters for use in the preliminary design [31]. These response parameters are representative for flight conditions an aircraft of this type might encounter during a typical mission.

The gust loads are calculated according to the certification specifications CS 23.341 for normal aircraft [32]. Using the

Pratt formula (6), gusts are translated to an equivalent load factor. The loads are then calculated as static maneuvers. More detailed information can be found in the NACA report 1206 [33].

$$n_z = 1.0 \pm \frac{k_g \cdot \delta_0 \cdot U_{de} \cdot V \cdot \left(\frac{dCl}{d\alpha}\right)}{2 \cdot \left(\frac{W}{S}\right)} \tag{6}$$

with:

k_g = gust alleviation factor

δ_0 = density of air at sea level

U_{de}= derived gust velocities

V = equivalent air speed

$\frac{dCl}{d\alpha}$ = lift curve slope

$\frac{W}{S}$ = wing loading

These load cases are calculated for all five mass configurations, see Table 2, for design cruise and design dive speeds V_c/ M_c and V_d/ M_d and at various Flight Levels (FL = altitude [ft] / 100), shown in Figure 7. The design cruise speed is Mach 0.8 at sea level and increases to Mach 0.9 at FL 75 while design dive speed is Mach 0.9 at sea level and increases to Mach 0.97 at FL 55. Finally, landing loads are calculated using the DLR in-house tool LGDesign [34] based on analytical formula and handbook methods. The maximum dynamic attachment loads of the landing gear are introduced into the structure as an additional load case. All in all, 216 load cases are taken into account.

4.2. Optimization Model

The objective is to minimize the structural weight while keeping the responses such as element strains inside their boundaries. The task is treated as a mathematical optimization problem and is formally defined in equation (7). Therein, f is the objective function with vector x containing the design variables and g is the constraint vector.

$$Min\{f(x)|g(x) \leq 0;\ x_{lower} \leq x \leq x_{upper}\} \tag{7}$$

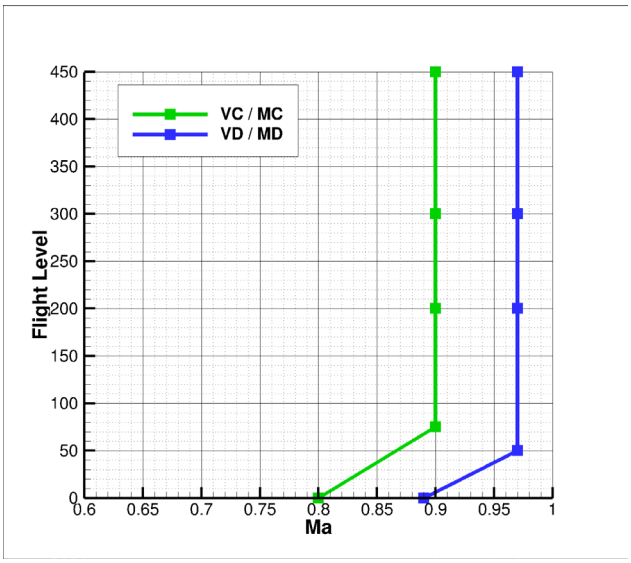

Figure 7: V_c/ M_c and V_d/ M_d envelope and flight points for the considered load cases

With 1200 µm/m (0.12 %) allowable compression and 1500 µm/m (0.15 %) allowable tension, derived from the material properties for unidirectional layers [25], the boundaries are rather conservative and provide a margin for possible changes in the configuration later. Currently, material thickness of upper and lower skin, spars and ribs are defined as optimization variables. The elements are grouped in areas and linked in order to define one variable per area. Therefore, the element with the highest strains governs the whole area. The structural model is designed in such a way, that left and right side have the same propertys, whereby the corresponding design areas are changed simultaneously, too. This is to ensure symmetry, a necessity when unsymmetrical load cases are considered. Summing up, the optimization problem has 168 design variables. The 6758 design responses multiplied by 216 load cases lead to ~1.5 Mio constraints.

It turns out that the optimization loops converge rather quickly and only two or three loops are necessary. However, experience has shown that there is no clear convergence in the sense of a function developing towards a

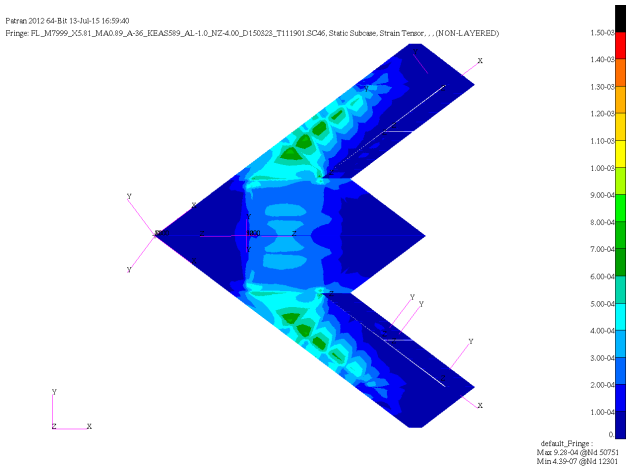

Figure 8: Element strain for, initial setup

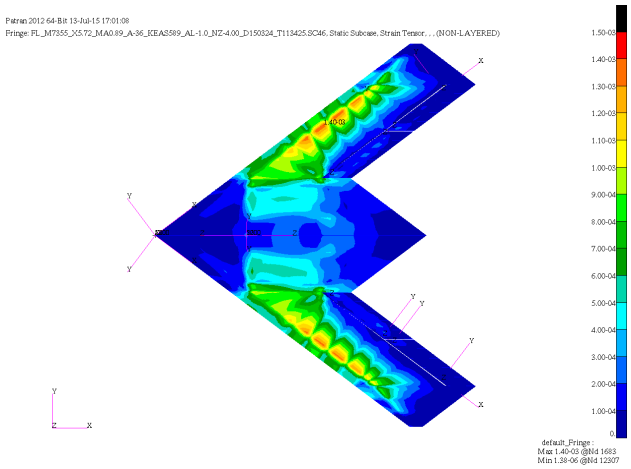

Figure 9: Element strain, after optimization

relative change of the objective function less than 0.001, the default value for MSC.Nastran SOL200. Instead, the results jump in a range of +/- 100 kg. This is acceptable for such kind of optimization and makes only 2-3 % of the final structural weight. Starting with an initial setup (uniform material thickness), the pure structural weight dropped to a final weight of 2750 kg. In order to compare the final result with the initial setup, the strain distribution is displayed for one load case in Figure 8 and Figure 9. After the optimization, the strains have nearly doubled and reach the upper limit of 1500 µm/m. In addition, they are distributed more evenly among the skin elements, suggesting a more efficient use of the material available.

5. LOADS ANALYSIS

5.1. General Aspects

The resulting structural model is used to conduct a comprehensive loads analysis campaign. The load cases and calculations are basically the same as for the sizing. While for the sizing nodal loads were required, now the emphasis lies on so-called interesting quantities. Interesting quantities usually include cutting forces and moments at various stations (e.g. along the wing or fuselage) and attachment loads (e.g. from control surfaces, payload, landing gear, etc.). The extraction of these quantities is done with the help of monitoring stations. The monitoring stations used in this work are taken from a collaboration with the Airbus Defence & Space loads department [35]. Difficulties are to find clear cuts of the structure and to avoid overdetermined regions due to unknown load paths e.g. at the control surface hinges or in the payload bay. Also, the choice of the coordinate systems is important. A local coordinate system with its y-axis along the leading edge provides more physically meaningful and understandable section forces and moments for the wing than a global coordinate system. However, with cuts in flow direction, a small “negative” area occurs that counteracts for example the moment about the x-axis.

The equations of motion solved for the static maneuver calculation is given in equation (8). The stiffness matrix K and the mass matrix M are multiplied by flexible deformations and rigid body motions u as well as accelerations $\ddot{u}$. Aerodynamic forces due to structural deformations are introduced by matrix Q. Finally, they are related to a vector of applied forces and moments P. The calculation is conducted with the reduced structural degrees of freedom a (a-set in MSC.NASTARN [36]).

$$(K_{aa} - q_\infty \cdot Q_{aa}(Ma)) \cdot \{u_a\} + M_{aa} \cdot \{\ddot{u}_a\} = \{P_a\} \tag{8}$$

The underlying equation of motion for dynamic gust calculation is given in equation (9) and differs from the static case. First, it is performed in modal coordinates h. In addition, matrix Q now depends on Mach number Ma and reduced frequency k and includes unsteady aerodynamic effects. The aerodynamic loads due to a discrete 1-cosine gust shapes are applied via $P_h(\omega)$.

$$\left(-M_{hh}\omega^2 + K_{hh} - q_\infty \cdot Q_{hh}(Ma,k)\right) \cdot \{u_h\} = \{P_h(\omega)\} \tag{9}$$

5.2. Maneuvering Loads

In Figure 10 and Figure 11 the three major cutting loads F_z, M_x and M_y due to manoeuver load cases are plotted for the wing root. They are plotted as two-dimensional load envelopes as far as combinations of the cutting loads lead to the maximum strains. In Figure 10 one can see that Fz has its highest amplitude in the negative region. This has several reasons. First, the wing is twisted negatively towards the outer regions. Secondly, for a positive angle of attack, the control surfaces deflect upwards to compensate the pitching moment. This upward deflection reduces the lift on the wing even further. Hence, for most horizontal flight conditions only the fuselage generates positive lift while the wing generates negative lift.

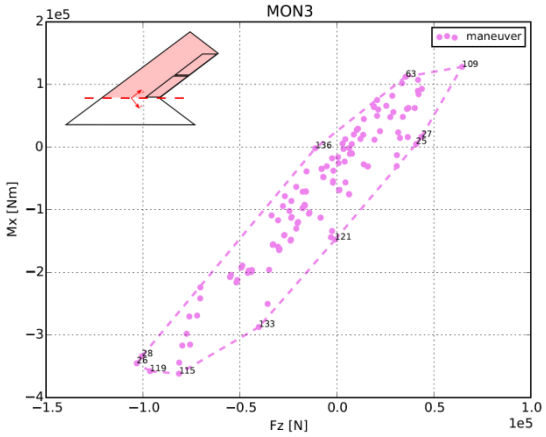

Figure 10: Cutting forces F_z and moments M_x at the wing root (MON3) for maneuver loads

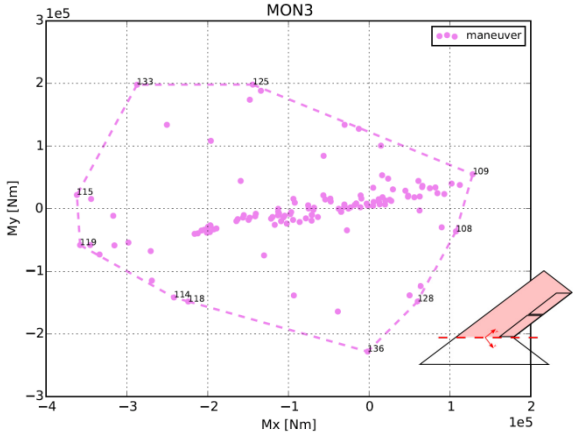

Figure 11: Cutting moments M_x and M_y at the wing root (MON3) for maneuver loads

The sign and amplitude of M_y changes significantly with the manoeuvers. Both high load factors N_z and roll rates/accelerations lead to large control surface deflections which cause a negative moment about the y-axis for upward and a positive moment for downward deflections. As expected, the highest manoeuver loads are caused by the design manoeuvers which combine high load factors

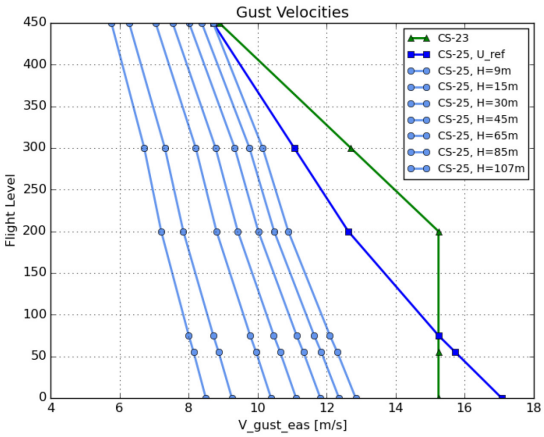

Figure 12: Assumed gust velocity profiles for Pratt and 1-cosine gusts

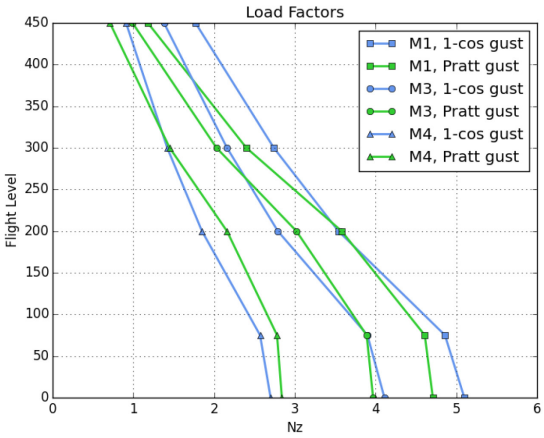

Figure 13: Load factors N_z obtained from Pratt and 1-cosine calculations

(N_z between -1.8 g and +4.5 g) with high roll rates / accelerations. The manoeuvers calculated according to CS 25.337 have lower load factors of -1.0 g and 2.5 g, thus showing lower loads.

5.3. Gust Loads

For the sizing of the DLR-F19 structure, the Pratt formula was applied to account for the gust loads. Now, a dynamic gust analysis is performed according to the certification specifications CS 25.341 for large aircraft [30]. The aircraft is exposed to a series of vertical 1-cosine shaped gusts with lengths H of 9, 15, 30, 45, 65, 85 and 107 m, both positive and negative and at the same altitudes, speeds and with the same mass configurations as before. Finally, the results are superposed with loads of a 1.0 g horizontal level flight.

For the Pratt formula, both wing area and aircraft weight are input parameters. As the wing area is rather large in comparison to the aircraft weight, the highest calculated load factors are 1.0 g ± 4.7 g (at sea level, lightest mass configuration M1). First, one can compare the resulting load factors from the dynamic 1-cosine simulation by summing up all inertia forces and dividing by the aircraft weight. It turns out the dynamic 1-cosine simulation produces not necessarily smaller load factors, but in general they are lower at lower altitudes and higher at higher altitudes. This can be explained by looking at the underlying gust velocities shown in Figure 12. The green curve is derived from CS 23.333 and used for the Pratt formula. The dark blue curve shows the reference gust velocities derived from CS 25.341. These reference gust velocities are further reduced by a flight profile alleviation factor and adapted to the gust length H, resulting in individual gust velocities for each gust length. In general, the gust velocities used for the Pratt formula are higher than those of the 1-cosine gust, with a peak at FL 200. With increasing altitude, the difference gets smaller. This trend is also reflected in the cutting forces. For academic purpose, one might correct these differences by simply using the same gust velocities for both types of calculations, as in [37].

A second observation is the tendency of Pratt load factors to be higher with increasing aircraft mass compared to 1-cosine gusts. In Figure 13 load factors N_z are plotted for both Pratt and 1-cosine gusts for mass configurations M1, M3 and M4. Once again, one can see a peak for Pratt load factors at Flight Level 200. But more important, for the lightest configuration M1, Pratt load factors are lower than those obtained from 1-cosine calculations. This is no longer the case for the heaviest configuration M4. Actually, this tendency is already discovered for mass configuration M3, where only a payload of two tons is added in comparison to M1. The reason for this effect could be explained by the gust alleviation factor k_g used in the Pratt formula, which might not be suitable for “flying wings” or aircraft with highly swept wings. The effect is represented in the loads plot in Figure 14 as well. Cutting forces F_z and moments M_x are plotted for a monitoring station at the wing root. Figure 14 shows that the loads in green obtained from Pratt are higher than those from the 1-cosine gust in blue. In fact, the highest cutting forces are produced by mass configuration M3. Looking at the cutting moments Mx and My in Figure 15, the Pratt loads are again higher than those from 1-cosine calculations. However, the area covered by the blue dots is much larger than the green area, indicating that higher torsional moments occur when performing a 1-cosine simulation. The explanation for this is that the 1-cosine simulations include structural dynamics while the Pratt calculations are quasi-static. This has for example a huge impact on the control surfaces, which are attached elastically to the fuselage as described in section 3.2. Taking a close look at the hinge forces and moment of the outer control surface in Figure 16, it is revealed the dynamic simulations lead to much higher hinge forces and moments than the quasi-static one.

6. CONCLUSION AND OUTLOOK

In this paper, the DLR’s parametric modelling process MONA is successfully used to create an aeroelastic model for a “flying wing” configuration. The resulting model is sized for 216 load cases including maneuver, gust and landing loads. The structural model is comparatively detailed for a pre-design phase and a model condensation is avoided. Together with a surface spline this is a very physical way of calculation aircraft loads that doesn’t require any loads reference axes. Also, new materials are employed as the aircraft is completely of carbon fiber composites.

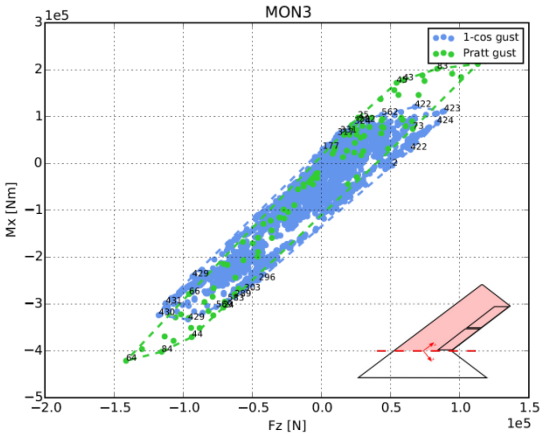

Figure 14: Cutting forces F_z and moments M_x at the wing root (MON3) for Pratt and 1-cosine gust loads

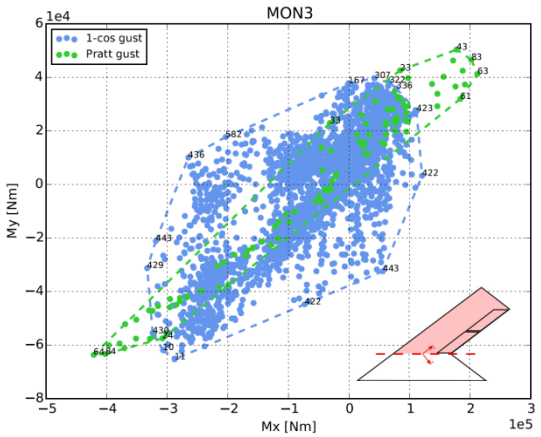

Figure 15: Cutting moments M_x and M_y at the wing root (MON3) for Pratt and 1-cosine gust loads

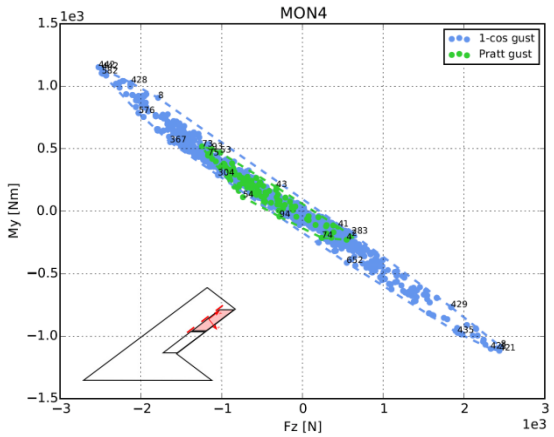

Figure 16: Hinge forces F_z and moments M_y of the outer control surface (MON4) for Pratt and 1-cosine gust loads

Once the model is sized, a comprehensive loads campaign is conducted. Next to maneuver loads, gust loads are calculated with both the quasi-static Pratt formula and the dynamic 1-cosine gust and compared. Differences can be explained by the different underlying gust velocities and by the gust alleviation factor. However, accounting for gust loads with the help of the Pratt formula is a good choice for a parametric modelling process that takes place in a pre-design phase. It might produce higher loads, but leaves a margin for later changes if the aircraft shall be certified according to CS-25.

In the future, aero-structural coupling could be improved by component-wise splining. Loads integration could be done by integrating aerodynamic forces directly, without splining them to the structure. This presumably results in an even better accuracy. The modelling of carbon fiber composites could be enhanced as well by modeling all individual plies instead of calculating engineering constants for the whole laminate setup. Doing that, one could also recognize the failure characteristics of carbon fiber composites in a more sophisticated manner and use them as constraints for the structural sizing. A lot of work was put into achieving the given center of gravity for the different mass configurations. However, the position of the center of pressure is rather vague, as the DLM is only valid for subsonic speeds. A shift of the center of pressure might change the trim results and therefore the loads could change significantly as well. A correction of the aerodynamic matrices might be necessary.

The authors wish to thank Georg Wellmer and Sara Kirchmayr from the Airbus Defence & Space loads department for the prolific collaboration.

REFERENCES

[1] K. C. Huber, D. D. Vicroy, A. Schuette, and A. Huebner, “UCAV model design and static experimental investigations to estimate control device effectiveness and Control capabilities,” presented at the 32nd AIAA Applied Aerodynamics Conference, Atlanta, GA, 2014.

[2] K. Huber, A. Schütte, and M. Rein, “Numerical Investigation of the Aerodynamic Properties of a Flying Wing Configuration,” presented at the 32nd AIAA Applied Aerodynamics Conference, New Orleans, Louisiana, 2012.

[3] K. Huber and A. Schütte, “Static and dynamic forces, moments and pressure distribution measurements on the DLR-F19 configuration,” DLR Institute of Aerodynamics and Flow Technology, Internal Report IB 124 - 2014/908, Jul. 2014.

[4] S. Wiggen and G. Voß, “Development of a wind tunnel experiment for vortex dominated flow at a pitching Lambda wing,” *CEAS Aeronautical Journal*, vol. 5, no. 4, pp. 477–486, 2014.

[5] C. M. Liersch and K. C. Huber, “Conceptual Design and Aerodynamic Analyses of a Generic UCAV Configuration,” presented at the 32nd AIAA Applied Aerodynamics Conference, Atlanta, GA, 2014.

[6] W. Krüger, S. Cumnuantip, and C. M. Liersch, “Multidisciplinary Conceptual Design of a UCAV Configuration,” in *Proceedings AVT-MP173*, Sofia, Bulgaria, 2011.

[7] “X-47B UCAS Unmanned Combat Air System Data Sheet.” Northrop Grumman Aerospace Systems, 2014.

[8] "X-47B UCAS Makes Aviation History…Again!," *Northrop Grumman*. [Online]. Available: http://www.northropgrumman.com/Capabilities/X47BUCAS/Pages/default.aspx. [Accessed: 25-Aug-2015].

[9] "Boeing Phantom Works to Lead Research on X-48B Blended Wing Body Concept - May 4, 2006." [Online]. Available: http://boeing.mediaroom.com/2006-05-04-Boeing-Phantom-Works-to-Lead-Research-on-X-48B-Blended-Wing-Body-Concept. [Accessed: 25-Aug-2015].

[10] "X-48B BWB Team Completes Phase 1 Test Flights," *NASA*, 05-Jun-2013. [Online]. Available: http://www.nasa.gov/centers/dryden/news/NewsReleases/2010/10-12.html. [Accessed: 25-Aug-2015].

[11] R. T. Britt, S. B. Jacobson, and T. D. Arthurs, "Aeroservoelastic Analysis of the B-2 Bomber," *Journal of Aircraft*, vol. 37, no. 5, pp. 745–752, Sep. 2000.

[12] B. A. Winther, D. A. Hagemeyer, R. T. Britt, and W. P. Roden, "Aeroelastic Effects on the B-2 Maneuver Response," *Journal of Aircraft*, vol. 32, no. 4, pp. 862–867, Jul. 1995.

[13] J. Schweiger, O. Sensburg, and H. J. Berns, "Aeroelastic Problems and Structural Design of a Tailless CFC-Sailplane," presented at the Second International Symposium on Aeroelasticity and Structural Dynamics, Aachen, 1985.

[14] "AK-X | Akaflieg Karlsruhe," *AK-X Ein moderner Nurflügel*. [Online]. Available: https://www.akaflieg.uni-karlsruhe.de/project/ak-x/. [Accessed: 17-Jul-2015].

[15] D. Chen, R. Britt, K. Roughen, and D. Stuewe, "Practical Application of Multidisciplinary Optimization to Structural Design of Next Generation Supersonic Transport," presented at the 13th AIAA/ISSMO Multidisciplinary Analysis Optimization Conference, Fort Worth, Texas, 2010.

[16] De La Garza, McCulley, Johnson, Hunten, Action, Skillen, and Zink, "Recent Advances in Rapid Airframe Modeling at Lockheed Martin Aeronautics Company," presented at the RTO-MP-AVT-173 Workshop, Bulgaria, 2011.

[17] Kelm, Läpple, and Grabietz, "Wing primary structure weight estimation of transport aircrafts in the predevelopment phase," presented at the 54th Annual Conference of Society of Allied Weight Engineers, Inc., Huntsville, Alabama, 1995.

[18] J. Wenzel, M. Sinapius, and U. Gabbert, "Primary structure mass estimation in early phases of aircraft development using the finite element method," *CEAS Aeronautical Journal*, vol. 3, no. 1, pp. 35–44, Apr. 2012.

[19] H. Tianyuan and Y. Xiongqing, "Aerodynamic/Stealthy/Structural Multidisciplinary Design Optimization of Unmanned Combat Air Vehicle," *Chinese Journal of Aeronautics*, vol. 22, no. 4, pp. 380–386, Aug. 2009.

[20] R. Nangia and M. Palmer, "A Comparative Study of UCAV Type Wing Planforms - Aero Performance & Stability Considerations," presented at the 23rd AIAA Applied Aerodynamics Conference, Toronta, Ontario, Canada, 2005.

[21] S. Woolvin, "A Conceptual Design Studies of the 1303 UCAV Configuration," presented at the 24th Applied Aerodynamics Conference, San Francisco, California, 2006.

[22] T. Klimmek, "ModGen User's Manual," Software Documentation, 2014.

[23] T. Klimmek, "Parametric Set-Up of a Structural Model for FERMAT Configuration for Aeroelastic and Loads Analysis," *Journal of Aeroelasticity and Structural Dynamics*, no. 2, pp. 31–49, May 2014.

[24] W. Krüger, T. Klimmek, R. Liepelt, H. Schmidt, S. Waitz, and S. Cumnuantip, "Design and aeroelastic assessment of a forward-swept wing aircraft," *CEAS Aeronautical Journal*, vol. 5, no. 4, pp. 419–433, 2014.

[25] M. Hanke, "DLR Projekt Mephisto Strukturkonzept," presented at the Mephisto Projektsitzung III-2014, Köln, 18-Nov-2014.

[26] H. Schürmann, *Konstruieren mit Faser-Kunststoff-Verbunden*. Berlin; Heidelberg; New York: Springer, 2007.

[27] W. P. Rodden and Albano, "A Doublet Lattice Method For Calculating Lift Distributions on Oscillation Surfaces in Subsonic Flows," presented at the AIAA 6th Aerospace Sciences Meeting, New York, 1968.

[28] Institute of Aerodynamics and Flow Technology, "DLR - TAU: Code description." [Online]. Available: http://tau.dlr.de/code-description/. [Accessed: 11-Aug-2015].

[29] R. L. Harder and R. N. Desmarais, "Interpolation using surface splines.," *Journal of Aircraft*, vol. 9, no. 2, pp. 189–191, Feb. 1972.

[30] European Aviation Safety Agency, Ed., *Certification Specifications for Large Aeroplanes CS-25*. 2015.

[31] G. Wellmer and S. Kirchmayr, "F19 SACCON - Response Parameters for Preliminary Design," TAECA42, Airbus Defence and Space GmbH, Memorandum, Mar. 2015.

[32] European Aviation Safety Agency, Ed., *Certification Specifications for Normal, Utility, Aerobatic, and Commuter Category Aeroplanes CS-23.* 2012.

[33] K. G. Pratt and W. G. Walker, "A Revised Gust-Load Formula and a Re-evaluation of V-G Data Taken on Civil Transport Airplanes From 1933 to 1950," NACA, Report 1206, 1953.

[34] S. Cumnuantip, "An Analytical Landing Gear Conceptual Design and Weight Estimation Program Description (LGDesign)," Software Documentation.

[35] G. Wellmer and S. Kirchmayr, "F19 SACCON – Monitor Station Positions," TAECA42, Airbus Defence and Space GmbH, Memorandum, May 2015.

[36] MSC.Software Corporation, "Set Definition," in *MSC Nastran Linear Static Analysis User's Guide*, vol. 2012.2, D. M. McLean, Ed. 2012, pp. 485–489.

[37] V. Handojo and T. Klimmek, "Böenlastanalyse der vorwärts gepfeilten ALLEGRA-Konfiguration," presented at the Deutscher Luft- und Raumfahrtkongress 2015, Rostock, 2015.